Hyperfine interactions in ^{61}Ni with synchrotron-radiation-based perturbed angular correlations

I. Sergueev,[1,*] O. Leupold,[1,†] H.-C. Wille,[1,2] T. Roth,[1] A. I. Chumakov,[1] and R. Rüffer[1]
[1]*European Synchrotron Radiation Facility (ESRF), P.O. Box 220, F-38043 Grenoble, France*
[2]*Hamburger Synchrotronstrahlungslabor (HASYLAB), DESY, D-22603 Hamburg, Germany*
(Received 23 August 2008; revised manuscript received 7 December 2008; published 31 December 2008)

We report on the observation of perturbed angular γ-γ correlations with 67.41 keV nuclear resonance of ^{61}Ni using nuclear resonance scattering of synchrotron radiation. The dependence of the correlations on the direction and the magnitude of the hyperfine magnetic field is demonstrated in the feasibility study with nickel metal. The interpretation of the experimental data is done using modification of the theory of conventional perturbed angular correlations for the case of the linearly polarized first photon.

DOI: 10.1103/PhysRevB.78.214436 PACS number(s): 76.80.+y, 23.20.En, 75.50.Cc

I. INTRODUCTION

The transition elements iron and nickel play an important role in human life and attract a large scientific interest. One of the methods which allows one to study chemical, structural, and magnetic properties of compounds containing these elements is Mössbauer spectroscopy (MS). Application of this method to study hyperfine interactions in iron using ^{57}Fe isotope is explored in many fields of science.[1,2] On the other hand, study of nickel by MS with ^{61}Ni isotope is used very rarely due to several technical and fundamental problems.[3] One of the technical issues, the short lifetime of the Mössbauer source, can be overcome using a time analog of MS, nuclear forward scattering (NFS) of synchrotron radiation. Several approaches[4,5] have been developed recently to perform NFS with ^{61}Ni.

Another obstacle of MS and NFS with the ^{61}Ni isotope is the high energy of the nuclear transition, which leads to small probability of the Mössbauer effect, i.e., the small value of Lamb-Mössbauer factor, even at low temperature. Investigations at ambient or higher temperatures become extremely difficult or even impossible, which strongly restricts an application of the methods.

The new method of synchrotron-radiation-based perturbed angular correlations[6,7] (SRPAC) does not depend on the Lamb-Mössbauer factor and allows one to extend investigations to the region where MS and NFS cannot be applied. SRPAC explores the spatially incoherent channel of nuclear resonant scattering. It can be considered as a scattering variant of time differential perturbed angular correlations[8,9] (TDPAC). In TDPAC the intermediate nuclear level is populated from above via a cascade of preceding nuclear transitions after decay of a radioactive parent. In SRPAC, on the contrary, the level is excited from the ground state via incoherent nuclear resonant scattering of synchrotron radiation. Directional selection and timing by the first detector in TDPAC are replaced in SRPAC by the direction and the timing of the incident flash of synchrotron radiation.

SRPAC has been briefly considered theoretically in the late 1970s as one of two (spatially coherent and incoherent) channels of nuclear resonant scattering.[10] The experimental demonstration of the method becomes possible with the advent of the powerful third generation synchrotron-radiation storage rings of European Synchrotron Radiation Facility (ESRF), APS, and SPring-8. The first study of the magnetic quantum beats in the incoherent-scattering channel has been performed with iron.[6] Recently, the application of SRPAC to study quadrupole interactions and relaxation in soft condensed matter has been demonstrated for the case of iron containing ferrocene molecules inserted into a glass former[7] and for the case of tributyltin fluoride polymer[11] containing the Mössbauer isotope ^{119}Sn.

In the present study we have applied SRPAC to investigate magnetic hyperfine interactions for the Mössbauer isotope ^{61}Ni. The study has been performed at room and higher temperatures, i.e., in the region where the Lamb-Mössbauer factor is negligible and conventional MS cannot be applied.

In Sec. II we compare dependence of two channels of nuclear resonance scattering, NFS and SRPAC, on the magnetic hyperfine interaction. The theoretical description of SRPAC in the presence of the magnetic hyperfine field is developed as a modification of the theoretical description of TDPAC for the case of the linearly polarized incoming photon. Finally, the analytical expression is given which describes the dependence of SRPAC on direction of the magnetic field and of scattering.

The experimental observation of the correlations from the nickel metal is presented in Sec. III. The dependence of the method on the scattering geometry and direction of magnetic alignment is demonstrated. The sensitivity of the method to the magnetic field is shown by measurements at different temperatures up to the Curie temperature of nickel metal. The main features and advantages of SRPAC with ^{61}Ni are summarized in conclusion and possible applications of the method to other high-energy Mössbauer isotopes are discussed.

II. THEORETICAL DESCRIPTION

The splitting of the nuclear states by hyperfine interactions leads to the interference of the scattering amplitudes with slightly different energies giving rise to the quantum beats in the nuclear resonant scattering. The quantum beat pattern is, however, different for the coherent and incoherent channels of the nuclear resonant scattering measured on the same ensemble of nuclei.

In Fig. 1 the energy-level diagram for the nuclear transition in ^{61}Ni is shown. This is $M1$ transition from ground

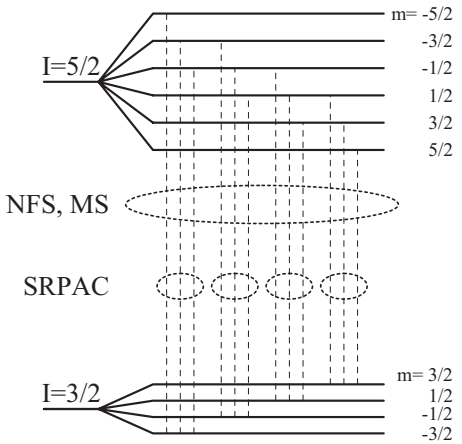

FIG. 1. Energy-level diagram for the nuclear transition in ^{61}Ni splitted by magnetic hyperfine interaction. The paths of scattering which interfere and give quantum beats are shown by circles for coherent (NFS) and incoherent (SRPAC) nuclear resonance scattering.

(spin 3/2) to excited (spin 5/2) state with small amount of $E2$ contribution which we will neglect in the following. The magnetic splitting leads to the 12 possible transitions from the ground to the excited state.

The spatial coherence of nuclear forward scattering implies that the nuclear system returns to its original state after scattering, i.e., the ground state of each nucleus is the same before and after scattering. Thus, there are 12 possible channels of scattering which are summed up on the amplitude level because of distribution of scattering over nuclear ensemble.[10]

Incoherent scattering takes place when a state of a particular nucleus after the scattering process is different from the original state; then the nucleus on which the scattering occurred can be identified. Also the ground nuclear state can be distinguished for this nucleus. The only indistinguishable paths of scattering are related to the different sublevels of the excited nuclear state through which scattering occurs. There are three possible channels of scattering which interfere and give rise to the quantum beat pattern in SRPAC. This pattern depends on the splitting of only excited nuclear state in contrast to NFS which also depends on splitting of the ground state.

The theoretical description of the time and angular dependences of SRPAC can be derived using the concept of perturbation factors that describe the time evolution of the intermediate excited nuclear state. This approach is used also in TDPAC. The important distinction of SRPAC is that the synchrotron-radiation photon is linearly polarized whereas in directional TDPAC the photons are assumed to be unpolarized. Here we limit the consideration to the $M1$ nuclear transition and static magnetic hyperfine interactions which perturb the nuclear states. The values of spin for the ground and excited nuclear states are not fixed in the following derivation, so that this approach can be applied to the different Mössbauer isotopes as ^{57}Fe, ^{61}Ni, and ^{119}Sn. The theoretical derivation of the expression for the scattering intensity for $M1$ nuclear transition gives[7]

$$I(t) = I_0 e^{-t/\tau_0}[1 - 2A_{22}R(t)], \tag{1}$$

where τ_0 is the lifetime of the excited state and A_{22} is the anisotropy coefficient equal to 0.14 for the $3/2 \rightarrow 5/2$ transition in ^{61}Ni and to 0.25 for the $1/2 \rightarrow 3/2$ transition in ^{57}Fe. All information about time and angular correlations are contained in the anisotropy factor $R(t)$. In the case of random orientations of the nuclear magnetic moments, $R(t)$ factorizes into angular and time dependent terms

$$R(t) = P_2(\cos\,\vartheta)G_{22}(t), \tag{2}$$

where the angular dependence is described by a second-order Legendre polynomial $P_2(\cos\,\vartheta)$ and the time dependence is described by the perturbation factor $G_{22}(t)$. The angle ϑ is the angle between the direction of the magnetic polarization $\mathbf{h}_1$ of the incoming photon and the direction of scattering for outcoming photon $\mathbf{k}_2$. The selection of $\mathbf{h}_1$ but not the direction $\mathbf{k}_1$ of the incoming photon as in TDPAC is related to the linear polarization of this photon. Usually, synchrotron radiation is polarized with $\mathbf{h}_1$ vertical to the plane of the synchrotron ring.

The perturbation factor $G_{22}(t)$ for hyperfine magnetic interaction is given as[12]

$$G_{22}(t) = \sum_{m,m'} \begin{pmatrix} I & I & 2 \\ m' & -m & m-m' \end{pmatrix}^2 e^{\imath\omega_B(m'-m)t}, \tag{3}$$

where m, m' denote sublevels of the excited state with spin I and $\omega_B = -g\mu_N B/\hbar$ is the Larmor frequency, proportional to the g factor of the nuclear excited state and to the magnetic field B. μ_N is the nuclear magneton. Formally $G_{22}(t)$ depends on the spin I, but after summation over m, m' this dependence disappears and Eq. (2) can be rewritten as

$$R(t) = P_2(\cos\,\vartheta)(1 + 2\,\cos\,\omega_B t + 2\,\cos\,2\omega_B t)/5. \tag{4}$$

The behavior of $R(t)$ for $\vartheta = 0$ is shown in the top part of Fig. 3.

Equations (2) and (4) are valid in the approximation of a random orientation of the nuclear magnetic moments over the sample. In the case of an alignment of the magnetic moments along the field $\mathbf{B}$, $R(t)$ in Eq. (1) can no longer be factorized to the angular and time dependent terms. In the Appendix we show that in this case the anisotropy is given as [Eq. (A6)]

$$R(t) = C_0 + C_1 \cdot \cos(\omega_B t - \Phi) + C_2 \cdot \cos(2\omega_B t - 2\Phi), \tag{5}$$

where C_0, C_1, and C_2 are

$$C_0 = (1 + 3\,\cos\,2\vartheta_0)(1 + 3\,\cos\,2\vartheta_2)/16,$$

$$C_1 = 3\,\sin\,2\vartheta_0\,\sin\,2\vartheta_2/4,$$

$$C_2 = 3(1 - \cos\,2\vartheta_0)(1 - \cos\,2\vartheta_2)/16. \tag{6}$$

The angles ϑ_0 and ϑ_2 between $\mathbf{B}$, $\mathbf{h}_1$, and $\mathbf{k}_2$ are shown in Fig. 2. Φ is the angle between the projections of $\mathbf{h}_1$ and $\mathbf{k}_2$ onto the plane perpendicular to $\mathbf{B}$. The sign of Φ is important and is defined by right-hand rule.

The anisotropy factor $R(t)$ in Eq. (5) consists of three terms: the time constant and two cosine-dependent terms of

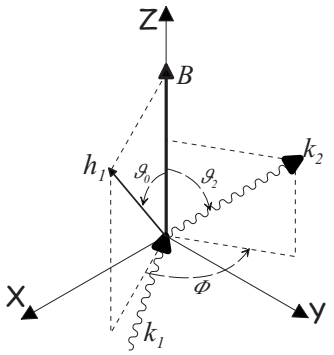

FIG. 2. Scattering geometry. Here **B** denotes the direction of the magnetic field; $\mathbf{k}_1$, $\mathbf{h}_1$ denote the direction and magnetic polarization of the incoming photon; $\mathbf{k}_2$ denotes the direction of the scattered photon.

the single and double Larmor frequencies. The weights of these terms are defined by the geometry of experiment. In particular, when the magnetic field is aligned along $\mathbf{h}_1$ or $\mathbf{k}_2$, then C_1 and C_2 in Eq. (6) are equal to 0 and $R(t)$ becomes time independent. There are no quantum beats in this case. If the magnetic field is normal to the plane formed by $\mathbf{h}_1$ and $\mathbf{k}_2$, then C_1 is equal to 0 and anisotropy is given as

$$R(t) = [1 + 3\cos(2\omega_B t - 2\Phi)]/4. \tag{7}$$

The behavior of $R(t)$ for such a geometry is shown in the middle part of Fig. 3 for $\Phi = 0$.

The phase of the quantum beats in SRPAC depends on sign of the angle Φ or, equivalently, on the direction of the magnetic field **B**. Inversion of this direction leads to a change of sign of Φ. A similar feature has been observed for the coherent nuclear Bragg scattering.[13] The sensitivity of SRPAC to the sign of the magnetic field suggests a simple way to distinguish between ferro- and antiferromagnetic alignments of the magnetic field in the sample. For the antiferromagnetic alignment the anisotropy is proportional to sum of two terms of Eq. (7) [or of Eq. (5) in the general case] with

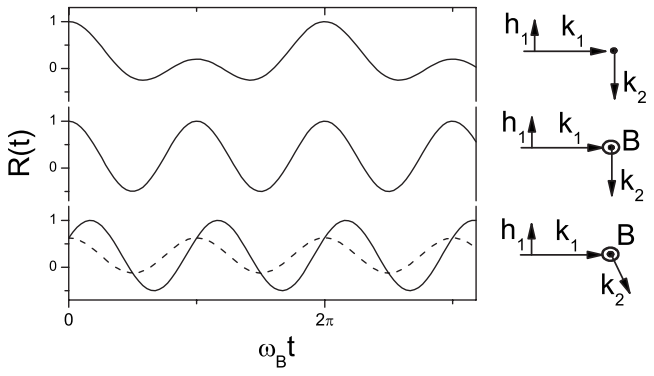

FIG. 3. Time dependence of the anisotropy $R(t)$: top—according to Eq. (4) for random orientation of magnetic field ($\vartheta = 0$); middle—according to Eq. (7) with magnetic field perpendicular to plane $\mathbf{h}_1$ and $\mathbf{k}_2$, ($\Phi = 0$); bottom—according to Eq. (7) (solid line) and Eq. (8) (dashed line) for ferro- and antiferromagnetic alignments ($\Phi = 30°$) of magnetic field, respectively.

Φ and $-\Phi$. Then we obtain for an antiferromagnetic alignment

$$R(t) = (1 + 3\cos 2\Phi \cdot \cos 2\omega_B t)/4, \tag{8}$$

where phase of the quantum beats becomes independent of Φ. The angle Φ defines here the contrast of the beats. The behavior of $R(t)$ for the ferro- and antiferromagnetic alignments according to Eqs. (7) and (8) is shown in the bottom part of Fig. 3 for $\Phi = 30°$ as an example. Thus, it is possible to separate the ferro- and antiferromagnetic alignments of the magnetic field in the sample from study of the phase of the quantum beats in the specific geometry of scattering.

III. EXPERIMENTS

The experiment was carried out at the nuclear resonance beamline[14] ID18 of the ESRF. The filling mode of the storage ring was the 16-bunch mode with a time window of 176 ns. The 67.4 keV incident radiation was monochromatized by a high-heat-load Si(3 3 3) double-crystal monochromator together with a 1 mm Cu absorber to suppress the 22.5 keV radiation passing via the Si(1 1 1) reflection. The flux of the transmitted radiation was about 4×10^9 photons/s in the bandwidth of ~9 eV. This bandwidth well covers the region of 100 meV around resonant energy which is significant for SRPAC due to the probability of scattering with absorption and emission of phonons.

The time evolution of the scattered radiation was monitored by a 10×10 mm^2 Si avalanche photodiode[15] with a thickness of 100 μm mounted in various positions around the sample at a distance of 10–20 mm from the sample. Such a distance was chosen to have an optimal compromise between an increase of the contrast of the beats and a decrease of the count rate when increasing the distance between the detector and the sample.

The detector was covered by 1 mm Al foil in order to suppress the 7.5 keV K_α radiation of the nickel atom produced by internal conversion. Probability of internal conversion is small due to small conversion coefficient, $\alpha = 0.13$. However, sensitivity of the Si photodiode to 7.5 keV radiation is 83%, much higher than the 0.63% sensitivity to the 67.4 keV resonant fluorescence. Therefore, the suppression of the 7.5 keV radiation is necessary.

We investigated SRPAC for a metal Ni foil enriched to 85% in the resonant isotope ^{61}Ni. The thickness of the sample along the beam was ~1 mm which corresponds to the absorption length of 67.4 keV radiation. A small external magnetic field was applied to the sample in order to introduce a defined magnetic orientation. Measurements were done at room temperature, where the Lamb-Mössbauer factor is $f_{\mathrm{LM}} \simeq 0.004$. Therefore, the possibility of recoilless scattering, which can strongly perturb the SRPAC signal,[7] is negligible. The count rate measured after 8 ns of the synchrotron pulse was of the order of 30 photons/s.

In order to investigate the time-angular correlations a set of measurements was performed at room temperature with different directions of the magnetic field and with different directions of the scattering. The sketches of the experimental geometries are shown in the right side of Fig. 5. The time

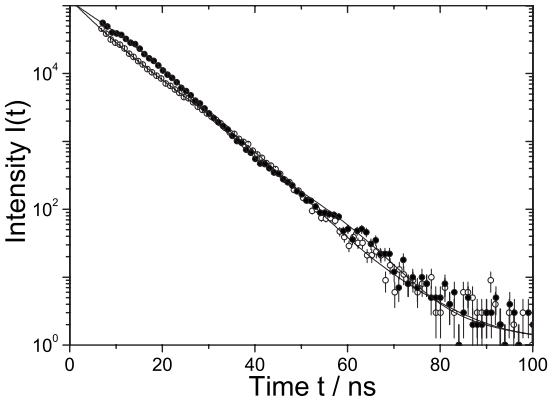

FIG. 4. Time evolution of the intensity (in log scale) for two directions of scattering. Open and filled circles correspond to geometry of Figs. 5(a) and 5(c), respectively. The solid lines are fits by Eqs. (1) and (7).

dependence of the intensity of scattering in the directions shown in Figs. 5(a) and 5(c) is presented in Fig. 4. The signal follows an exponential decay in time modulated by quantum beats due to the magnetic hyperfine interaction. The period of these beats is around 50 ns. The rotation of the detector by 90° changes phase of the beats to opposite.

The fit of the data has been performed using Eqs. (1) and (5) where the experimental geometry was taken into account. The lifetime of the excited state of ^{61}Ni obtained from the fit is $\tau_0 = 7.54 \pm 0.03$ ns which is consistent with the reported value[16] of 7.7 ± 0.2 ns. The anisotropy coefficient A_{22} varies for different measurements between 0.09 and 0.12 depending on the distance between the detector and the sample. This value is smaller than the theoretical value of 0.14 due to the average over the solid angle covered by the detector.

The anisotropy factor $2A_{22}R(t)$ obtained from the experimental data using Eq. (1) is shown in Fig. 5 for five different geometrical setups. Except the last one, all setups correspond to the case when the magnetic field **B** is normal to the plane of the magnetic polarization $\mathbf{h}_1$ of the incoming photon and of the direction of scattering $\mathbf{k}_2$. Therefore, Eq. (7) can be used to describe these data. The beat structure is defined by cosine-type oscillations with the frequency equal to the double Larmor frequency and with the phase equal to the double angle between $\mathbf{h}_1$ and $\mathbf{k}_2$. In particular, a 90° rotation of $\mathbf{k}_2$ between Figs. 5(a) and 5(c) and Figs. 5(b) and 5(d) changes phase to opposite. Figure 5(e) shows the case when **B** is parallel to $\mathbf{h}_1$, which leads to the complete suppression of the beats. This suppression does not depend on the direction of the scattering, which was checked also experimentally. It is important to point out the principal difference between conventional (directional) TDPAC and SRPAC with linearly polarized incoming radiation. In directional TDPAC, the beats are suppressed when **B** is parallel to $\mathbf{k}_1$ [Fig. 5(b)] while in SRPAC in this geometry beats are seen. On the other hand, in the setup of Fig. 5(e) beats would be seen with TDPAC and they are not seen in SRPAC.

The sensitivity of SRPAC to the change of the magnitude of the hyperfine field has been studied in a second set of measurements. Here, the scattering from nickel has been observed at various temperatures from room temperature up to

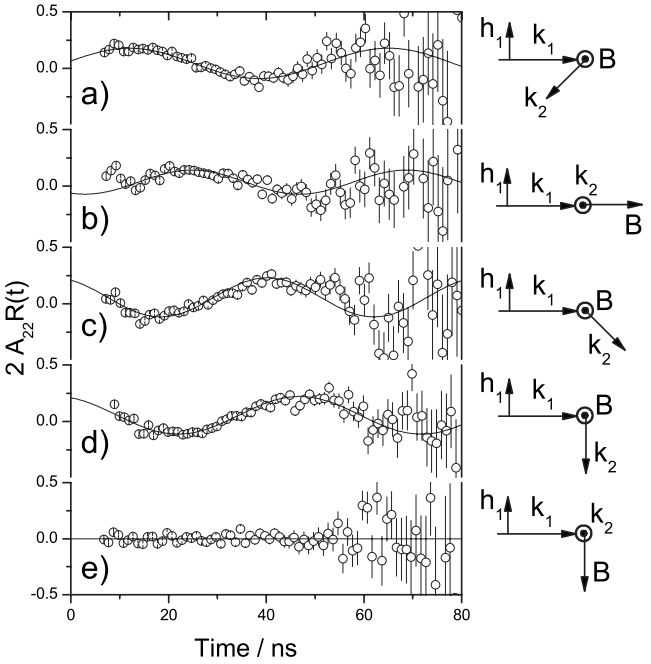

FIG. 5. Time evolution of the anisotropy factor $2A_{22}R(t)$ for various configurations of the magnetic field and scattering directions. The sketches of experimental setup are shown on the right side. The peak in the data around 55 ns seen in Figs. 5(a)–5(c) is artificial and due to the reflection in the detector electronics.

the Curie temperature $T_C = 630$ K. The nickel foil was installed in a furnace together with magnets for the magnetic alignment. The geometrical setup was the same as in Fig. 5(d) with the distance between sample and detector of about 15 mm. The typical acquisition time was about 2–3 h for one spectrum.

The time dependence of the anisotropy factor $2A_{22}R(t)$ for various temperatures is shown in Fig. 6. The frequency of the beats decreases with the increase of temperature and at 635 K, i.e., at 5 K above Curie temperature, the beats disappear and data are described by a simple exponential decay which corresponds to constant value of $2A_{22}R(t)$. The fit of the entire set of the data was done with the same value of the lifetime τ_0 which was obtained from data at 635 K and with the same value of the anisotropy coefficient A_{22} which was obtained from data at 300 and 375 K. Anisotropy factor was fitted using Eq. (7) with $\Phi = 0$ due to geometrical setup. However, it was found that above 500 K the contrast of the beats is significantly smaller than for low temperatures. Because A_{22} is fixed by the experimental setup, which is the same for all temperatures, the only way to explain this decrease is to assume a certain kind of additional exponential damping

$$R(t) = \tfrac{1}{4}\exp(-\lambda t/\tau_0)[1 + 3\cos(2\omega_B t)], \qquad (9)$$

where λ is the damping rate. The physical origin of this damping is not clear. It may have a dynamical nature due to spin relaxation. Also, we can explain this damping by the temperature gradient in the sample which produces a distribution of the hyperfine field. Another explanation can be

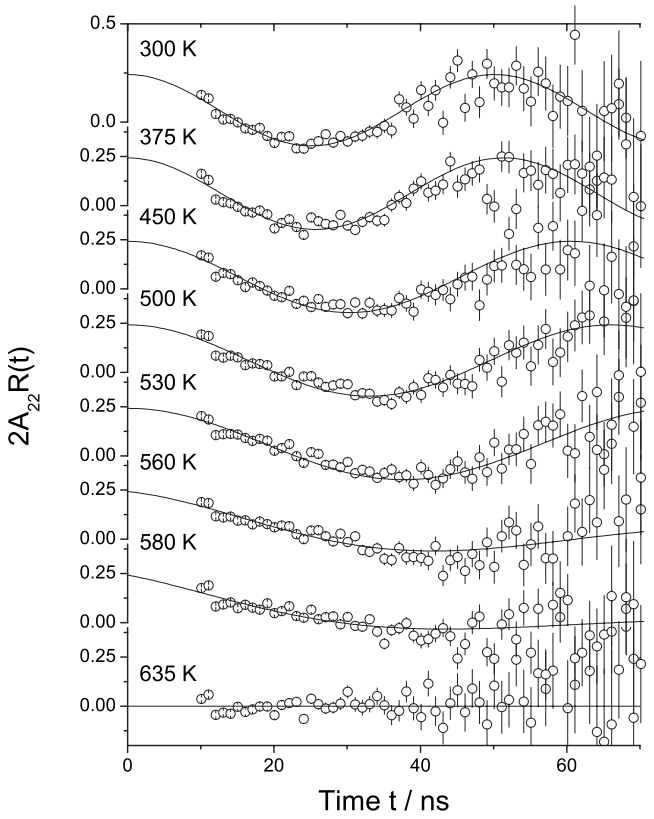

FIG. 6. Time evolution of the anisotropy factor $2A_{22}R(t)$ for several temperatures. The solid lines are fit according to the theory.

related to the distribution of the magnetic orientation at high temperatures. In this case the damping in Eq. (9) has to be applied only to the oscillating term. However, this modification leads only to the scaling factor in the damping rate and does not change quality of the fit of our data. Because only part of the period of the quantum beat is observed above 500 K, all these processes can explain the experimental data. We should remark that the additional damping term in the anisotropy factor is not unusual and is used in TDPAC to describe relaxation processes or distributions.

The temperature dependence of the magnetic field obtained by SRPAC is shown in Fig. 7. For comparison, the magnitude of the hyperfine magnetic field measured by NMR (Refs. 17 and 18) is shown. There is good agreement between the two data sets. It is seen that SRPAC for ^{61}Ni allows one to measure magnetic hyperfine field down to 3–4 T. The damping rate is shown in the inset of Fig. 7. It becomes visible above 500 K and increases up to 0.2 at 580 K.

IV. CONCLUSION

In this paper we applied the method of SRPAC to investigate hyperfine interaction with ^{61}Ni, a Mössbauer isotope with a high-energy nuclear transition. The study has been performed in the temperature range where the probability of the Mössbauer effect is negligible and other methods such as Mössbauer spectroscopy or nuclear forward scattering of synchrotron radiation cannot be applied.

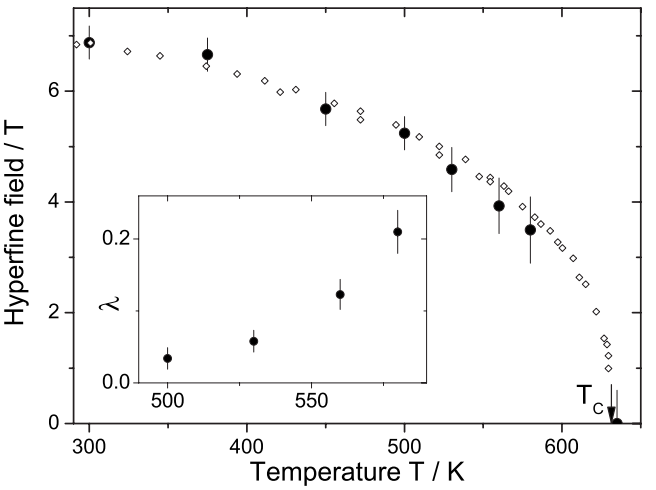

FIG. 7. Temperature dependence of the hyperfine magnetic field in nickel as measured by SRPAC (●) and NMR (◇) (Refs. 17 and 18). Inset: temperature dependence of the damping rate λ [see Eq. (9)].

The observation of SRPAC with metal nickel at various geometries of scattering and of the magnetic field and at different temperatures allows one to investigate the methodical aspects of the method. Thus, in this experiment the feasibility to study hyperfine interactions in nickel is demonstrated.

The theoretical description of SRPAC in the presence of a magnetic field is in general similar to the description of conventional TDPAC but with important modifications due to the linear polarization of the first (incoming) photon. Based on the general description of SRPAC for $M1$ nuclear transition, we here developed the theory which describes SRPAC for the case of magnetic hyperfine interaction. The obtained theoretical approach can be applied to any Mössbauer isotope with the spin value of the excited state larger than 1/2, in particular to ^{61}Ni and to ^{57}Fe splitted by magnetic hyperfine interaction. It was also found theoretically that SRPAC is a convenient method to distinguish between ferro- and antiferromagnetic alignments of the sample.

The further development of the method has to be done in the direction of increasing the efficiency of detectors and optimization of the monochromator. In the presented experiment only ~0.04% of the total resonance fluorescence were recorded. By taking several detectors which cover a larger solid angle and which would have better efficiency to 67.4 keV radiation, one can increase the count rate drastically. Additionally, the optimization of the monochromator can give at least a factor of 10 in flux. Such improvements would allow one to apply SRPAC to study hyperfine interactions in the compounds with small concentrations of the ^{61}Ni isotope.

The independence of SRPAC on the Lamb-Mössbauer factor makes the method convenient to study hyperfine interactions in other high-energy Mössbauer isotopes as well. In particular, it looks promising to apply SRPAC to study hyperfine interactions in the rare-earth Mössbauer isotopes with a nuclear transition from spin 0 to spin 2. The examples of such isotopes are ^{160}Gd, ^{168}Er, and ^{174}Yb. The properties of those nuclear transitions lead to a very large beat contrast in

the range of unity because of the additional fourth order term in the expansion of the scattering intensity in Eq. (1). Therefore, even while the lifetime of the excited state is small (around 3 ns), the beats would be well pronounced and information about hyperfine interactions can be obtained.

APPENDIX: CALCULATION OF SRPAC FOR MAGNETIC INTERACTION

According to Ref. 7 the scattering intensity of SRPAC for the $M1$ nuclear transition is given as

$$I(t) = I_0 e^{-t/\tau_0}[1 - 2A_{22}R(t)], \tag{A1}$$

$$R(t) = \sum_{qq'} D^{(2)}_{0q}(\mathbf{h}_1 \rightarrow \mathbf{S}) G^{qq'}_{22}(t) D^{(2)}_{q'0}(\mathbf{S} \rightarrow \mathbf{k}_2), \tag{A2}$$

where $D^{(2)}_{0q}(\mathbf{h}_1 \rightarrow \mathbf{S})$ denotes Wigner D functions (rotation matrix elements), $\mathbf{h}_1$, $\mathbf{S}$, and $\mathbf{k}_2$ are unit vectors along the magnetic polarization of the incoming photon, the quantization axis of hyperfine interactions, and the direction of the scattered photon, respectively. For a static magnetic interaction the perturbation coefficients $G^{qq'}_{22}(t)$ are easily obtained in the coordinate system with z axis along the magnetic field $\mathbf{B}$ as a rotation around this axis [see Eq. (13.156) in Ref. 12]

$$G^{qq'}_{22}(t) = \delta_{qq'} D^{(2)}_{qq}(-\omega_B t, 0, 0), \tag{A3}$$

where ω_B is the Larmor frequency. Inserting Eq. (A3) into Eq. (A2) we obtain

$$R(t) = \sum_q D^{(2)}_{0q}(\mathbf{h}_1 \rightarrow \mathbf{B}) D^{(2)}_{qq}(-\omega_B t, 0, 0) D^{(2)}_{q0}(\mathbf{B} \rightarrow \mathbf{k}_2)$$
$$= D^{(2)}_{00}[\mathbf{h}_1 \rightarrow \mathbf{B}(-\omega_B t) \rightarrow \mathbf{k}_2] = P_2[\cos\ \eta(t)], \tag{A4}$$

where $\mathbf{h}_1 \rightarrow \mathbf{B}(-\omega_B t) \rightarrow \mathbf{k}_2$ is the rotation from direction of $\mathbf{h}_1$ into $\mathbf{B}$, then the rotation about $\mathbf{B}$ by an angle $-\omega_B t$, and then the rotation into the direction $\mathbf{k}_2$. $P_2[\cos\ \eta(t)]$ is the second-order Legendre polynomial and $\cos\ \eta(t)$ is the normalized scalar product of $\mathbf{h}_1$ and $\mathbf{k}_2$ modified by the change of coordinate system in time. In the coordinate system related to $\mathbf{B}$, where ϑ_0, ϑ_2 and ϕ_0 and ϕ_2 are the polar and azimuthal angles of $\mathbf{h}_1$ and $\mathbf{k}_2$, respectively, we obtain

$$\cos\ \eta(t) = \cos\ \vartheta_0 \cos\ \vartheta_2 + \sin\ \vartheta_0 \sin\ \vartheta_2 \times \cos[\omega_B t - (\phi_2 - \phi_0)]. \tag{A5}$$

Inserting Eq. (A5) into the Legendre polynomial in Eq. (A4) and simplifying we arrive at

$$R(t) = \frac{1}{16}(1 + 3\cos 2\vartheta_0)(1 + 3\cos 2\vartheta_2) + \frac{3}{4}\sin 2\vartheta_0 \sin 2\vartheta_2 \cdot \cos(\omega_B t - \Phi) + \frac{3}{16}(1 - \cos 2\vartheta_0)(1 - \cos 2\vartheta_2) \cdot \cos(2\omega_B t - 2\Phi), \tag{A6}$$

where Φ is defined as $\phi_2 - \phi_0$.

*sergueev@esrf.fr

†Also at Hamburger Synchrotronstrahlungslabor (HASYLAB), DESY, D-22603 Hamburg, Germany.

[1] For an introduction, see, e.g., G. K. Wertheim, *Mössbauer Effect: Principles and Applications* (Academic, New York, 1964).

[2] For recent applications, see, e.g., the Proceedings of the ICAME Conference [Hyperfine Interact., Vol. 165 (2005)]; Proceedings of the ICAME Conference [Hyperfine Interact., Vol. 156/157 (2004)].

[3] C. A. McCammon, Can. J. Phys. **65**, 1294 (1987).

[4] T. Roth, O. Leupold, H.-C. Wille, R. Rüffer, K. W. Quast, R. Röhlsberger, and E. Burkel, Phys. Rev. B **71**, 140401(R) (2005).

[5] I. Sergueev, A. I. Chumakov, T. H. Deschaux Beaume-Dang, R. Rüffer, C. Strohm, and U. van Bürck, Phys. Rev. Lett. **99**, 097601 (2007).

[6] A. Q. R. Baron, A. I. Chumakov, R. Rüffer, H. F. Grünsteudel, and O. Leupold, Europhys. Lett. **34**, 331 (1996).

[7] I. Sergueev, U. van Bürck, A. I. Chumakov, T. Asthalter, G. V. Smirnov, H. Franz, R. Rüffer, and W. Petry, Phys. Rev. B **73**, 024203 (2006).

[8] H. E. Mahnke, Hyperfine Interact. **49**, 77 (1989).

[9] T. Butz, Z. Naturforsch., A: Phys. Sci. **51**, 396 (1996).

[10] G. T. Trammell and J. P. Hannon, Phys. Rev. B **18**, 165 (1978).

[11] C. Strohm, I. Sergueev, and U. van Bürck, Europhys. Lett. **81**, 52001 (2008).

[12] R. M. Steffen and K. Alder, *The Electromagnetic Interaction in Nuclear Spectroscopy* (North-Holland, Amsterdam, 1975).

[13] D. E. Brown, J. Arthur, A. Q. R. Baron, G. S. Brown, and S. Shastri, Phys. Rev. Lett. **69**, 699 (1992).

[14] R. Rüffer and A. I. Chumakov, Hyperfine Interact. **97**, 589 (1996).

[15] A. Q. R. Baron, Hyperfine Interact. **125**, 29 (2000).

[16] M. R. Bhat, Nucl. Data Sheets **88**, 417 (1999).

[17] M. Rotter and B. Sedlak, Czech. J. Phys., Sect. A **20**, 1285 (1970).

[18] M. Shaham, J. Barak, U. El-Hanany, and W. W. Warren, Phys. Rev. B **22**, 5400 (1980).